Biorheology 38 (2001) 119–142
IOS Press

A new view of mechanotransduction and strain amplification in cells with microvilli and cell processes

Sheldon Weinbaum *, Peng Guo and Lidan You
Department of Mechanical Engineering and Center for Biomedical Engineering, The City College of New York, New York, NY 10031, USA

Received 5 February 2001
Accepted in revised form 29 March 2001

Abstract. In this paper we shall describe new mechanical models for the deformation of the actin filament bundles in kidney microvilli and osteocytic cell processes to see whether these cellular extensions, like the stereocilia on hair cells in the inner ear, can function as mechanotransducers when subject to physiological flow. In the case of kidney microvilli we show that the hydrodynamic drag forces at the microvilli tip are <0.01 pN, but there is a 38-fold force amplification on the actin filaments at the base of the microvilli due to the resisting moment in its terminal web. This leads to forces that are more than sufficient to deform the terminal web complex of the microvillus where ezrin has been shown to couple the actin cytoskeleton to the Na^+/H^+ exchanger. In the case of bone cell processes we show that the actin filament bundles have an effective Young's modulus that is 200 times $>$ the measured modulus for the actin gel in the cell body. It is, therefore, unlikely that bone cell processes respond *in vivo* to fluid shear stress, as proposed in [59]. However, we show that the fluid drag forces on the pericellular matrix which tethers the cell processes to the canalicular wall can produce a 20–100 fold amplification of bone tissue strains in the actin filament bundle of the cell process.

Keywords: Mechanotransduction, brush border microvilli, osteocytic cell processes, glomerulotubular balance, bone strain amplification

1. Introduction

In contrast to the actin cytoskeleton in the main body of the cell, where the actin network forms a gel-like structure that is isotropic, many cells have slender microvilli or cell processes in which the actin network is highly organized into cross-linked axial arrays or bundles in which the long axes of the actin filaments are parallel to one another. Four prominent examples of such structures are the brush border microvilli of the proximal tubule and small intestine, the hair cells of the inner ear and the cell processes on osteocytes. Except for the stereocilia on the hair cells in the inner ear, very little attention has been paid until recently for these actin filament bundles to serve as possible mechanotransducers that could either amplify strain or stress. This lack of association is due in large measure to the wide disparity in function of the cells and the organs in which the cells reside.

In this paper we will explore the mechanical deformation of the actin filament bundles in brush border microvilli and osteocytic cell processes to see whether these cellular extensions, like the stereocilia on

*Address for correspondence: Dr. S. Weinbaum, Dept. of Mechanical Engineering, The City College of New York, New York, NY 10031, USA. Fax: +1212 6506727; E-mail: weinbaum@ccny.cuny.edu.

hair cells, can function as mechanotransducers. In particular, we want to quantitatively examine whether these cells are capable of intracellular biochemical and/or electrical response in response to fluid flow under *in vivo* physiological conditions. This comparative study has been motivated by two recent papers by the author and coworkers [16,63], in which new mechanosensory hypotheses are introduced to explain glomerulotubular balance in the proximal tubule and a strain amplification mechanism that would enable bone cells *in vivo* to sense the very low amplitude strains in mineralized whole bone that occur at physiological loading.

This comparative study is also motivated by the fact that much more is known about the cytoskeletal structure of the actin filament bundles of brush border microvilli in the intestine and stereocilia than the equivalent structures in kidney microvilli and osteocyte cell processes. Both the cross-linking proteins in the filament bundles themselves and their terminal web have been well characterized in the intestine and, in the case of stereocilia, there is considerable information as to how the actin filament bundles deform. This information provides valuable insight in constructing structural mechanical models for kidney microvilli and bone cell processes where much less is known about the cytoskeletal structure. Rather surprisingly, there is only one prior study to our knowledge, Rodman et al. [46], that has examined the close parallel between brush border microvilli in the intestine and the kidney although structurally the microvilli closely resemble one another and their main function is transport. It is only very recently that the close similarity between the actin filament bundles in brush border microvilli and the osteocytic cell process has been pointed out [55]. Both have actin filament bundles with the same cross-linking molecules, fimbrin and α-actinin, and the diameters of their cellular extensions are nearly equivalent, 0.1 μm, although their lengths differ by an order of magnitude.

From a mechanotransduction viewpoint there is an intriguing contrast between the fluid mechanical forces acting on kidney microvilli and osteocytic cell processes. In kidney brush border microvilli the fluid flow is transverse to the microvilli and the primary mechanical force is the fluid drag on the microvilli tips. This hydrodynamic force produces a torque on the terminal web or cytoplasmic root of the filament bundle. In bone cells the fluid flow is directed along the axes of the cell processes and the principal force is either the shear force on the cell process membrane or the drag on the transverse fibers that attach the cell process to the mineralized canalicular wall. The brush border microvilli act as cantilever beams and the longer osteocytic cell processes, we shall show, act as suspended cables. Brush border microvilli are uniform in length, form a closely spaced hexagonal array, and are connected to one another and a surrounding occludens junction through a terminal web of cytoskeletal components at the base of the microvilli [12]. In contrast, osteocytic cell processes are heterogeneous extensions that are linked at their tip by gap junctions which provide for cell to cell communication [66].

It is intuitively obvious that the effective elastic modulus of a highly structured actin filament bundle is much larger than the isotropic actin gel in the cell body. The effective Young's modulus has been measured for stereocilia consisting of hundreds of actin filaments; however, to our knowledge there has been no prior attempt to calculate an effective Young's modulus for an actin filament bundle from first principles, that is the Young's modulus of an individual axial actin filament, the structural arrangement of the cross-linking molecules and how this composite structure deforms under mechanical forces. The stiffness of the actin filament bundle raises important questions about cellular signaling that have not, here-to-fore, been considered in numerous *in vitro* studies which have examined the effect of fluid shear stress on cells with cell processes or microvilli. These studies have been conducted in flow chambers where the cells have been subjected to fluid shear stresses of typically 5–30 dyn/cm^2. In this flow regime, investigators have observed a wide range of intracellular responses from an increase in intracellular Ca^{++} and various second messengers to the upregulation and expression of various genes [44,62]. *In vivo* it

is only the tips of the renal brush border microvilli and the membranes of the cell processes of bone cells that are subjected to fluid shears in this range and not the cell body itself. The model in You et al. [63] predicts that the effective Young's modulus for an actin filament bundle is at least two orders of magnitude greater than the isotropic actin gel in the cell body. This suggests that the fluid shear stress responses observed in cell culture arise from the deformation of the relatively soft actin cytoskeleton in the cell body and not the much stiffer actin filament bundle in their cellular extensions, which we propose are the actual sites of the mechanotransduction *in vivo* for both bone cells and proximal tubule epithelia.

2. Background

To provide a more detailed basis for comparison we shall first provide a brief description of the salient structural and functional features of the three basic types of cellular extensions, stereocilia, brush border microvilli and bone cell processes.

2.1. Stereocilia

The stereocilia on hair cells have been extensively studied because it is well recognized that they respond to acoustic waves and sense the directionality of linear and angular momentum needed for balance [22]. The stereocilia on the inner hair cells, which act as the primary receptor for the auditory system, have a highly specialized structure in which they are arranged in rows of ascending height, much like steps. The tips and upper lateral margins of adjacent stereocilia are cross-linked by thin filaments which connect neighboring stereocilia across rows in the direction of the steps [56], see Fig. 1. Hudspeth [22] also showed that deflections of the stereocilia across the rows in the direction of increasing height lead to ion channel opening and a depolarization of the cells, whereas a bending in the opposite direction led to a hyperpolarization. In contrast, bending along a row causes no electrical response. In the case of the hair cells this depolarization leads to neurotransmitter release at synapses where the afferent nerves carry electrical signals to the brain. A more detailed description of the electro-mechanical coupling and the difference in function between inner and outer hair cells can be found in reviews by Hackney and Furness [18].

Stereocilia for most species are intermediate in length (2–10 μm) between brush border microvilli (1.5–3.0 μm) and osteocytic cell processes (20–30 μm). They also differ from microvilli in that they significantly taper at their point of attachment to the cuticular plate. There can be several hundred actin filaments in the main body of the stereocilia, but only twenty or so of the central filaments form the root that penetrates the cuticular plate and becomes embedded in the cuticular matrix. This substantial taper allows the stereocilia to torsionally pivot at their base when they are subjected to mechanical forces at their tips. The actin filament structure of stereocilia and its cross-linking has been extensively studied by Tilney and co-workers in a series of papers summarized in Tilney and Tilney [57]. These authors show that the pattern of the cross-linking bands when the stereocilia is bent by a mechanical force applied at the tip of the tallest stereocilia in the staircase provides strong evidence that the filaments slide past one another much like the pages of a book. The periodic bands formed by the fimbrin cross-links remain parallel to the apical surface. This suggests that the fimbrin cross-links are highly flexible at their attachment points, inextensible and offer little resistance to axial bending. This observation is a critical input into the formulation of our elastic models for the bending of the brush border microvilli and the cell process.

Most mechanical models for the bending of the stereocilia [21,42] represent the stereocilia as rigid levers with torsional springs at their base and elastic gating springs at their tips. The gating spring, which

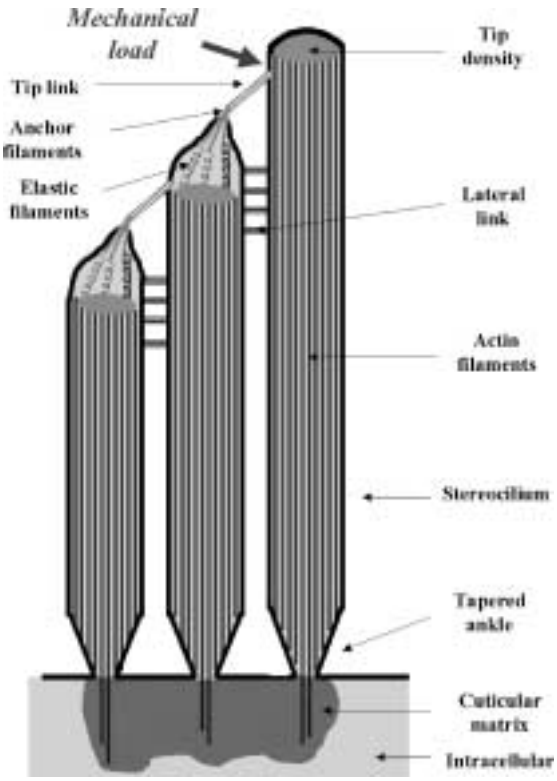

Fig. 1. Schematic cross section of stereocilia on one hair cell. Stereocilia are arranged in rows of ascending height, generating a staircase-like pattern. They are connected to each other by tip and lateral links. When a mechanical load is applied stereocilia pivot as a coupled unit about tapered ankles at their base. Each stereocilium contains several hundred closely spaced actin filaments except at their base where 20–30 form a root that enters the cuticular matrix.

is associated with the tip link filament, is critical to the mechano-electrical transduction. Hudspeth [23] has shown that they transmit a force that leads to the opening and closing of membrane ion channels that are in close proximity to the attachment site at the stereocilia tip. A very recent study on the structure of the hair cell tip links, Kachar et al. [24], suggest that the tip links are rigid filaments and that the elastic component arises from the tent-like membrane deformation of the microvillus tip at the point of tip attachment above a densely stained region called the tip density, see Fig. 1. The three fundamental structural differences between stereocilia and brush border microvilli, which we consider next, are that there are no visible cross linking filaments between adjacent microvilli, their heights are remarkably uniform, and there is no taper of the actin filament bundle at its point of entry into the cell body. Stereocilia have an ankle which permits torsional rotation of the stereocilia at their base which is absent in microvilli.

2.2. Brush border epithelia

Superficially, there would appear to be a close similarity between the brush border microvilli in the small intestine and the kidney. Both have microvilli of roughly the same dimensions, 0.1 μm diameter. and 2 μm length, which are arranged in a regular hexagonal array. However, from a structure–function viewpoint, the small intestine and the proximal tubule differ greatly although both have transport as their principal function. The microvilli on the apical surface of the epithelial cells of the intestinal villi are

essentially shielded from the movement of the chyme in the lumen of the intestine by the protruding villi, which are convoluted and themselves closely packed. The chyme is driven by a slow peristaltic motion and it is only the digestive juices that slowly seep across the intestinal microvilli. The fact that the microvilli in the small intestine are shielded from flow makes it unlikely that these brush border microvilli function as flow stimulated mechanotransducers.

In contrast to the microvilli in the small intestine, the microvilli in the proximal tubule are directly exposed to the fluid flow in the lumen of the convoluted proximal tubule, see Fig. 2. Figure 2A is a schematic showing the cross-section of a convoluted tubule epithelial cell and Fig. 2B is a sketch of the tubule cross-section showing the direction of the brush border microvilli. The most striking feature of these microvilli is their uniformity in height and regularity of spacing. The most important unsolved mystery in the functioning of the proximal tubule is the afferent mechanism in "glomerulotubular balance". Why is it that no matter how much fluid is filtered in the Bowman capsule, the fractional reabsorption of water and small ions in the proximal tubule remains nearly constant at approximately 65%. The fundamental unanswered questions are (i) how do the brush border epithelial cells sense the magnitude of the fluid flow in the lumen, what is the mechanotransducer, and (ii) how is this mechanical signal converted into a chemical response that that controls the entry of Na^+ at the apical surface that is need to replenish the active transport of Na^+ on the basolateral surfaces.

The axial actin filament structure of the proximal tubule microvilli was first observed by Hassen and Hermann [19]. Subsequent studies [36,47] showed that each microvillus contains a distributed array of 6–8 axial filaments of 7 nm diameter which subsequent immunochemical analysis showed were F-actin [3]. There is a very close correspondence between the structural components of the cytoskeleton of the brush border microvilli in the intestine and proximal tubule [46]. This organization is especially well characterized for the small intestine, see Fig. 3 adapted from Furukawa and Fechheimer [12] and Mooseker and Tilney [37]. The cross-linking proteins that contribute to the bundle formation are villin and fimbrin, although fimbrin is less prominent in the kidney microvilli [46]. In the intestine the membrane of the microvillus is tethered to the actin bundle by a double helical spiral of protein linkages that have been identified as brush border myosin I [33]. These lateral myosin links on which the membrane rests are periodically spaced at 33 nm intervals along the outer filaments of the actin bundle and create a circular annulus of 20–30 nm thickness between actin filament bundle and the microvillus membrane [37]. These lateral linkages have not yet been identified for kidney microvilli. The actin filaments have

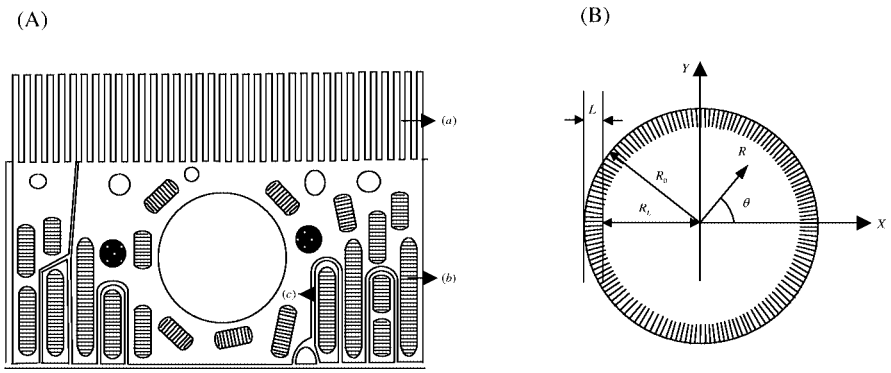

Fig. 2. (A) Schematic diagram of an epithelial cell in proximal tubule S2 segment. The cells in this segment are characterized by densely spaced microvilli of uniform height (a), numerous mitochondria (b), and extensive interdigitation of the lateral membrane near the basal surface (c). (B) Idealized mathematical model of tubule cross-sectional geometry, with brush border of thickness L.

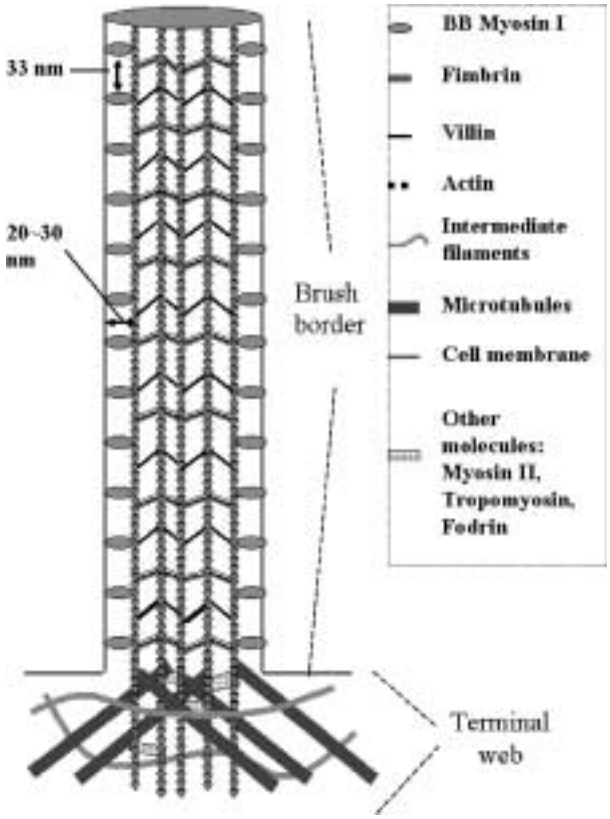

Fig. 3. Sketch of cytoskeleton inside an intestinal microvillus. The intracellular structure of the intestinal microvillus is composed of two regions, a brush border and a terminal web.

a directionality with a barbed end at the apex and a base that is attached to a terminal web of linker molecules. These linker molecules, tropomysin, fodrin and myosin II, attach the microvilli to a supporting structure of intermediate filaments and microtubules and also to actin filaments associated with the adherens junction.

There are several structural differences between the brush border microvilli in the intestine and the kidney which strongly suggest a difference in function as a possible mechanotransducer. The actin filament bundle in the intestine is significantly stiffer (30 axial actin filaments compared to 6–8 in the kidney), the microvilli are more closely spaced (nearly touching in the intestine compared to a 74 nm open gap at control flow conditions in the kidney) and the kidney epithelia have numerous clathrin coated pit regions which make for a more rigid supporting structure at the microvillus base [46]. The closely spaced microvilli in the intestine can easily touch one another during peristaltic contractions, whereas the microvilli in the kidney, we shall show, undergo only small non-contacting displacements at their tips.

2.3. Osteocytes

Osteocytes in bone tissue have long slender cell processes whose diameter is comparable to the diameter of microvilli, but whose length (20–30 μm) is an order of magnitude greater, see electronmicrograph in Fig. 4. These processes are housed in long tubes in the mineralized matrix called canaliculi whose diameter is about twice that of the cell processes. The space between the canalicular wall and the cell

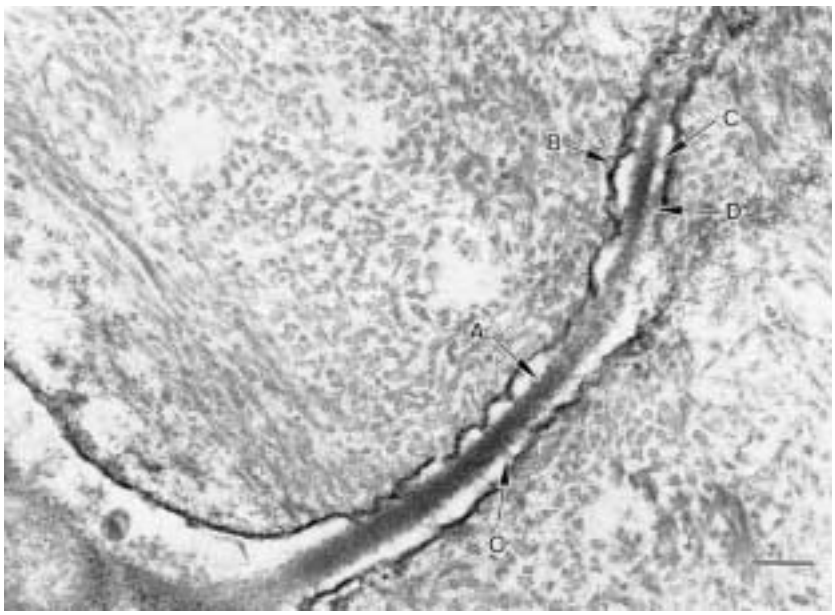

Fig. 4. Electron micrograph of the longitudinal section of an osteocyte cell process in a canaliculus. A, process; B, canalicular wall; C, transverse elements; D, pericellular matrix. Bar, 0.2 μm, $\times$56 400.

process membrane is a fluid annulus that contains pericellular matrix. The fundamental unanswered question in bone mechanotransduction is how the very small strains in whole bone (i.e., tissue level strains of 0.04–0.3%, [11]) can cause cellular signaling when bone cells in deformed cell cultures respond to strains that are typically 1% or larger [5,64]. One hypothesis that has obtained widespread support is that the deformation of the mineralized bone matrix due to mechanical loading produces a fluid flow in the lacunar-canalicular porosity that generates a shear stress on the cell process membrane [59]. *In vitro* studies in flow chambers support this hypothesis in that increases in intracellular Ca^{++} and other biochemical responses [44,62] are observed for shear stresses on the cell process membrane whose magnitude (5–30 dyn/cm^2) falls in the range predicted in [59]. This shear stress response is not only observed for bone cells but for all vascular endothelial cells. The counter intuitive prediction in [59], that attracted widespread interest, is that the predicted magnitude of the fluid shear stress on the osteocytic cell process membrane due to physiological loading is roughly of the same order as that on vascular endothelium where the effect of blood flow is much more obvious.

While the fluid shear stress hypothesis for bone cell stimulation is very appealing, two predictions in You et al. [63], described herein, seriously challenge this hypothesis and suggest an alternative explanation based on flow induced strain amplification. First, the theory in You et al. shows that the effective Young's modulus for an actin bundle is 200 fold larger than the actin gel in the body of the cell and, therefore, it is likely that in culture it is the actin cytoskeleton in the cell body that is responding to the shear stress rather than the much stiffer actin bundle in the cell process. In contrast, *in vivo* the cell body of the osteocyte lies within a lacuna that is surrounded by a pericellular matrix layer that is typically 1.0 μm thick and the shear stresses on the cell body are much smaller than those on the cell process membrane. Second, the theory in You et al. also predicts that the fluid drag force on the pericellular matrix that is attached to the cell process membrane is much greater per unit cell process length than the shear force on the cell process membrane just described. These contradictions have led to a new flow induced strain

amplification hypothesis in You et al. [63] in which the deformation of the actin filament bundle in the cell process is coupled to the fluid drag on the transverse tethering filaments in the pericellular matrix.

The fundamental questions raised in this section have led to the development of new models to explore the deformation of actin filament bundles in kidney brush border microvilli and bone cell processes. These new models and their quantitative predictions will now be described.

3. Model for proximal tubule microvilli

In Guo et al. [16] a new mechanosensory hypothesis is introduced to explain the afferent mechanism in "glomerulotubular balance". To examine this hypothesis quantitatively, Guo et al. have developed an elastohydrodynamic model to predict the forces and torques acting on each microvillus and the bending deformation that results from this hydrodynamic loading. The fluid flow model to determine the velocity distribution in the brush border, the slip velocity at its edge and the flow in the lumen is sketched in Fig. 2B. The model to determine the detailed flow past the individual microvilli and the local drag forces on each microvillus in the array is shown in Fig. 5. The basic hydrodynamic model is that of viscous flow in a circular tube whose wall is covered by slender protuberances of uniform height, $L = R_{\mathrm{o}} - R_{\mathrm{i}}$, arranged in an hexagonal array as illustrated in Fig. 5. This fluid flow geometry, where the microvilli are perpendicular to the tubule wall, is very difficult to treat because the flow near the tips of the microvilli is fully three-dimensional. There is a complicated fiber interaction layer near the edge of the brush border which leads to a slip velocity at the tips of the microvilli. The equivalent two-dimensional flow problem, where the circular cylinders in Fig. 5 are infinitely long, is described in a well known paper by Sangani and Acrivos [50]. In [16] a new solution approach is developed in which the velocity profiles in the tubule are first determined by applying effective medium theory (Brinkman equation) in the brush border region and the Navier–Stokes equation in the interior region, $R < R_{\mathrm{i}}$, the lumen of the tubule. The local value of the Darcy permeability K_{p} in the brush border that appears in the Brinkman equation is determined from the solution in [50] for the infinite cylinder array in Fig. 5.

The solutions for the axial velocity profile in the tubule are shown in Fig. 6 for a control tubule flow rate of 30 nl/min. The dimensions of the microvilli are based on the ultrastructural data in Maunsbach [35]. The length of the microvillus is 2.5 μm, its diameter is 90 nm, the luminal diameter of the tubule is 27.7 μm and the microvillus density is 42.5/μm^2, which corresponds to a microvillus spacing of $\Delta =$ 74.1 nm in Fig. 5. The velocity profile is broken into three regions in Fig. 6 since the velocity scales are

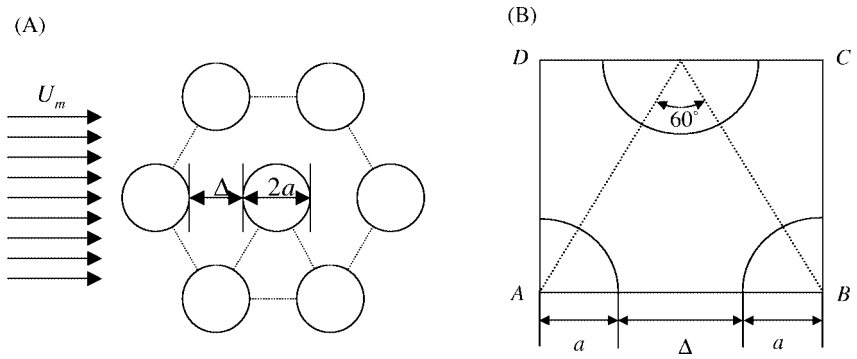

Fig. 5. (A) Idealized model of brush border in transverse section showing hexagonal microvillus array. (B) Repetitive periodic unit of the hexagonal microvillus array. Note that this unit contains the equivalent of one microvillus.

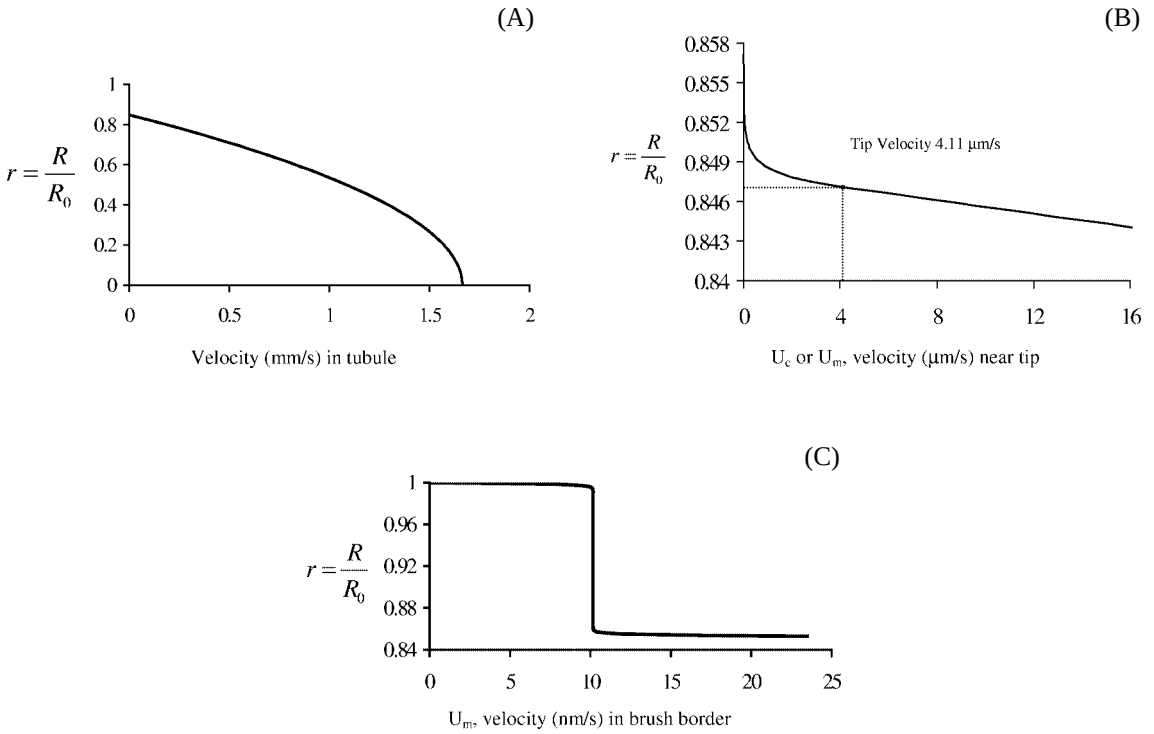

Fig. 6. Velocity profiles (A) in lumen, (B) in tip region and (C) in central region of brush border. Tip is located at $r = 0.847$. Note that velocity at microvilli tip is approximately $1/400$ the center line velocity in core and bulk flow in brush border is approximately $1/400$ of the tip velocity.

so different. Figure 6A is the central lumen, $R < R_{\mathrm{i}}$, where the velocity is a typical parabolic Poiseuille profile; Fig. 6B is the average velocity distribution in the fiber interaction layer in the vicinity of the microvilli tips which are located at a dimensionless radius $r = R/R_{\mathrm{i}}$ of 0.847; Fig. 6C is the velocity in the interior of the brush border. One notes that the average slip velocity at the edge of the brush border is 4.11 μm/s or $1/400$ of the maximum velocity, 1.66 mm/s, on the tubule centerline and that the velocity in the interior of the brush border away from the tip region is only 10 nm/s or ≈1/400 of this slip velocity. There are very thin fiber boundary layers of the order of the microvilli spacing, Δ, both at the apical membrane, $R = R_{\mathrm{o}}$, and at the edge of the brush border, $R = R_{\mathrm{i}}$. The one near the edge of the brush border is of special significance since it determines the axial flow velocity near the microvilli tips and hence the distribution of the drag force in this thin region. From a mass flow standpoint the flow in the brush border is vanishingly small due to the very small velocities in this region. This slow flow is driven by the axial pressure gradient in the tubule and not the shear forces imposed by the flow outside the brush border.

The force and torque distribution on the microvilli due to the hydrodynamic drag is subtle. The basic question is how the drag imposed by the nearly uniform very slow flow in the interior of the brush border, which acts over most of the microvillus length, compares with the drag on the microvillus in the thin fiber interaction region near its tip. To resolve this question we have applied a local two-dimensional theory to determine the drag per unit length on the microvillus. This local value of the drag scales linearly with the local average axial velocity shown in Fig. 6 and is obtained by examining the pressure drop across the

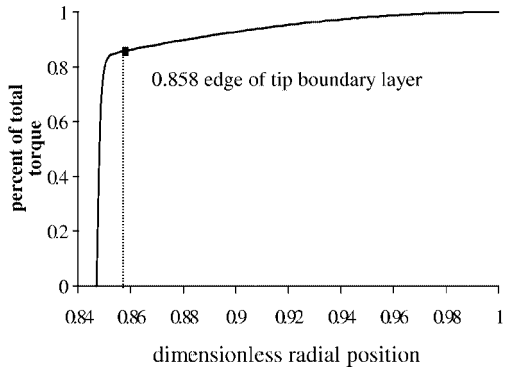

Fig. 7. Integrated torque distribution along the microvillus starting from the microvillus tip. Note that 86.2% of the total torque occurs in the tip interaction layer, outer 0.18 μm of microvillus near tip.

repetitive periodic unit that is sketched in Fig. 5B, namely, the average pressure drop from the border AD to the border BC. The results of this calculation show that 74% of the total drag occurs within 7% of the microvillus length near the tip, or the outer 0.18 μm of the brush border. This detailed drag distribution can then be used to determine the integrated torque distribution on the microvillus. The latter distribution is shown in Fig. 7. One starts at the microvillus tip, $r = 0.847$, and then integrates the product of the local drag per unit length times the local lever arm, which is measured from the base of the microvillus. One notes that at $r = 0.858$, the edge of the tip interaction layer (outer 0.18 μm of the brush border) this integrated torque is 86.2% of the total torque. This implies that $6/7$ of the total torque arises from the flow near the tip and $1/7$ from the flow in the interior of the brush border where the velocity profile in Fig. 6A shows that the velocity and hence the drag are uniform.

The force and torque distribution just described has been used to construct an idealized structural model for the bending of the microvillus, which is shown in Fig. 8. The microvillus is treated as a cantilever beam comprised of seven axial actin filaments which is rigidly attached to a terminal network of microtubules and intermediate filaments in the terminal web at its base as shown in the sketch in Fig. 3. This terminal network is envisioned to function much like the roots of a tree. The loading on the microvillus, see Fig. 8B, has two components, a uniformly distributed load q_{m} due the drag forces in the interior of the brush border, and a concentrated load P_{m} due to the integrated drag force acting in the thin fiber interaction layer near the tip (outer 0.18 μm). The cross-section of the beam is composed of seven parallel actin filaments which are arranged in a hexagonal array as shown in Fig. 8A. The cross-linking molecules have been shown in Rodman et al. [46] to be villin and to a lesser extent fimbrin. These cross-linking molecules are assumed to determine the actin filament spacing but have little effect on the bending stiffness, since we assume that the actin filaments can slide by one another as discussed earlier in the background section on stereocilia. Based on the electron micrographs in Maunsbach [36], the six off-center filaments are assumed to be located on the mid-radius of the microvillus section and the radius of each actin filament is taken as 3.5 nm. These dimensions are used to calculate the moment of inertia I of the cross-section. Simple beam theory is then used to calculate the deflection of the beam. The final result for the tip deflection $y(L)$ is

$$y(L) = \frac{1}{EI}\left(\frac{P_{\mathrm{m}}L^3}{3} + \frac{q_{\mathrm{m}}L^4}{8}\right). \tag{1}$$

Here L is the length of the beam and E is the Young's modulus of an individual F-actin filament.

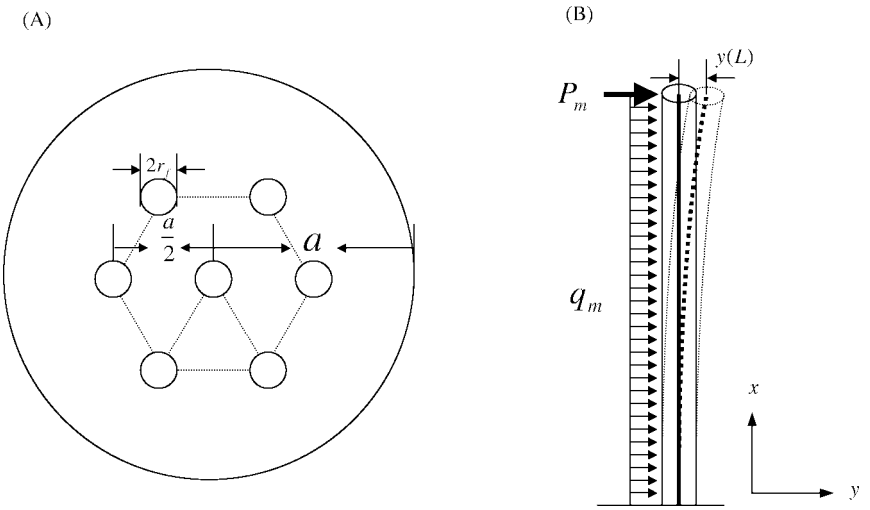

Fig. 8. (A) Idealized structural model for the arrangement of axial F-actin filaments in microvillus cross-section. The seven F-actin filaments form an hexagonal array in which the six off axis filaments are equally spaced on a circle that is the half radius of the cross-section. a is the radius of the microvillus membrane and r_f is the radius of the actin filament. (B) Geometry of the deformed microvillus showing axial deflection of its central filament. The mechanical loading is a combination of a concentrated force, P_m, acting at the tip, accounting for approximately three-quarters of the total drag force and a uniform loading, q_m, accounting for approximately one-quarter of the total drag force.

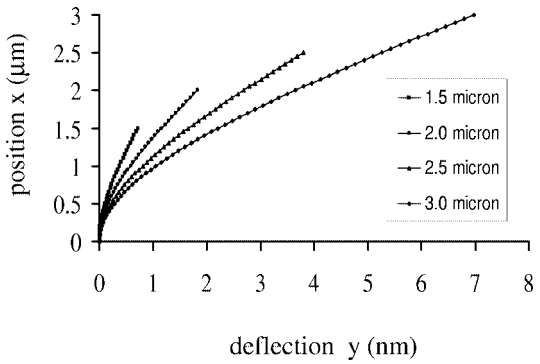

Fig. 9. Microvillus deflection for control flow, 30 nl/min, for microvilli of four different lengths from 1.5 to 3.0 μm. $2R_L = 27.7$ μm and $\Delta = 74.1$ nm for all microvilli.

The predicted bending deformation of the microvillus is shown in Fig. 9 for several microvilli ranging in length from 1.5 to 3.0 μm. Both P_m and q_m scale linearly with the flow rate Q in the tubule provided the tubule radius remains constant. The value for E has been determined by the micromanipulation of a single actin filament in Kishino and Yanagida [26]. The calculated value of E for this experiment, 1.44×10^9 dyn/cm^2, compares well with more recent techniques using optical tweezers [10]. The results shown are for $Q = 30$ nl/min. For this flow a 2.5 μm microvillus has a deflection of 3.8 nm at its tip. The tip displacement is about 5% of the 74 nm spacing between microvilli and thus the microvilli can be viewed as relatively stiff bristles which maintain their highly ordered hexagonal arrangement and do not touch one another at physiological flow rates. This behavior is required if the microvilli are to serve as mechanotransducers. The fluid drag on each microvillus tip for $Q = 30$ nl/min is remarkably small,

0.0074 pN, suggesting that a large amplification is needed if the actin cytoskeleton is to detect this signal. The integrated drag force on all the microvilli is approximately 30 pN per cell.

4. Model of osteocytic cell processes

In You et al. [63] a new hypothesis is proposed for cellular level flow induced strain amplification in the actin filament bundles of the osteocytic cell process. It has been recognized since the mid 1960's [58] that the fluid annulus surrounding the osteocytic cell process is filled with a pericellular matrix that occupies the entire space between the cell process membrane and the canalicular wall. This matrix is clearly evident in the electron micrograph shown in Fig. 4 where the canalicular wall is unusually sharply defined. The molecular components of this matrix are unknown, but there is strong evidence that it contains proteoglycan like molecules [1,51]. Weinbaum et al. [59] have proposed that the side chains of these molecules have a sieving structure that is similar to the endothelial glycocalyx which is known to selectively sieve albumin, 7 nm diameter. A similar sieve is needed in bone since the clefts of bone capillaries are known to be permeable to albumin and such a sieve would be required to prevent the leakage of albumin into bone tissue. Using this model for the pericellular matrix, Weinbaum et al. predicted from poroelastic theory that the shear stress on the cell process membrane for physiological loading was comparable to the shear stress on vascular endothelium. When this analysis was combined with electrokinetic theory in Cowin et al. [9], these authors were also able to obtain reasonable agreement for the measured phase and magnitude of the stress generated potentials (SGP) as function of frequency for *in vitro* bone specimens in four point bending [49,53].

The model proposed in You et al. [63] goes far beyond this initial model in Weinbaum et al. [59] for predicting the fluid shear stress on bone cell processes. It proposes a mechanism via which the pericellular matrix surrounding the cell process interacts with the actin filament bundle in the interior of the cell process and also predicts how the deformation of this extracellular matrix due to fluid flow can lead to large amplifications in bone tissue level strains in the actin cytoskeleton of the cell process. Before describing this model, we shall first examine the electronmicrographs in Figs 4 and 10 more carefully.

Two striking features in the electron micrograph in Fig. 4 are the stiff appearance of the cell process and its actin filament bundle, and the fact that the process follows a winding course through the canaliculus without ever making contact with the canalicular wall. This last observation is even more evident when one views the many canaliculi in transverse cross-section in Fig. 10. One observes that virtually all the cell processes are centrally located within the canaliculi. The authors surmised that such central positioning could not be achieved without the cell process being tethered by transverse extracellular fibers to the canalicular wall much like the vertical cables of a suspension bridge attach the roadway to its main suspending cables. The arrows in Fig. 4 illustrate several examples of this transverse tethering. Figures 4 and 10 are just two of many electron micrographs obtained by L. You in M. Schaffler's laboratory at Mt. Sinai School of Medicine. In other electron micrographs the authors have observed nearly periodic arrays of transverse spanning elements with a spacing of approximately 50 nm. The stiff appearance of the cell process in Fig. 4 is consistent with the calculation for the bending stiffness of brush border microvilli in the previous section.

The ultrastructural studies in Tanaka-Kamioka et al. [55] indicate that in cell culture the actin filament bundles of the osteocytes fill nearly the entire cross-section of the cell process and that these axial filaments are cross-linked by at least fimbrin and α-actinin. The α-actinin component is also present in the cell body where it forms an isotropic gel and it is the presence of the fimbrin that is essential for

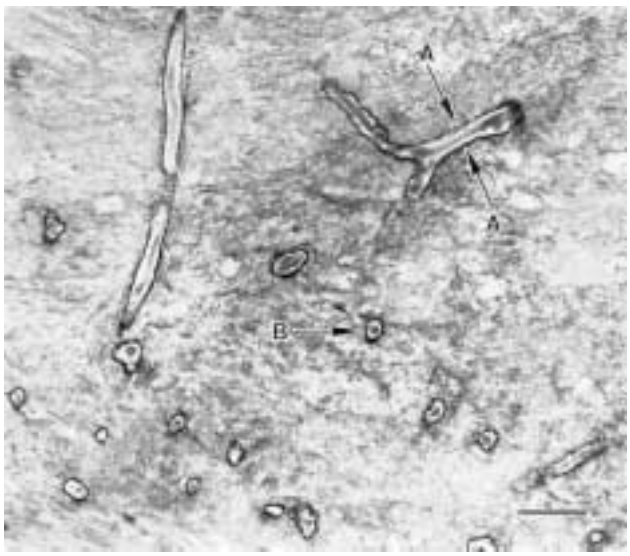

Fig. 10. Electron micrograph showing the cross sections of several osteocyte processes. The central positioning of the processes in the canaliculi can been clearly seen. A, Longitudinal section of a canaliculus showing cell process of its center. The black line is the canalicular wall. B, Transverse cross section of a canaliculus with cell process contained at its center. The black line along the outer circle is the canalicular wall. Bar, 1 μm, $\times$12780.

the bundle formation. The study by Tanaka-Kamioka et al. does not state whether the other important cross-linking protein, villin, which serves a central function in the assembly of the actin bundles in brush border microvilli is present. There is also no information on how the actin filament bundle is attached to the cell process membrane, but it is reasonable to assume that there are lateral linkages that are equivalent to the brush border myosin I linkages shown in Fig. 3.

The new hypothesis for strain amplification is illustrated by the four panel diagram in Fig. 11. Figure 11A is a sketch of the canalicular cross-section showing the transverse elements which tether the cell process to the canalicular wall. Possible candidates for the attachment molecules for this tethering are CD44, laminin and various integrins [14,40]. The shaded region surrounding each transverse element is a negatively charged matrix of glycosaminoglycans (GAG), which form the side chains or branches of the transverse elements. The negative charge causes the GAG to distend and form a hydrated gel with an osmotic swelling pressure. When the fluid moves along the axis of this fluid annulus it creates a drag on the GAG and a tension in and deformation of the transverse tethering elements as shown in Fig. 11B. Since this drag is uniformly distributed along the length of the transverse element, see Fig. 11D, the deformed shape is that of a catenary. This is the same shape as a hanging chain in a gravitational field where the loading is also uniform. The strain amplification mechanism is illustrated in Fig. 11C. The basic premise is that the tensile force on the transverse elements is first transmitted by CD44 or integrins across the cell process membrane and then transferred by lateral linker molecules, similar to brush border myosin I, to the actin filament bundle in the core of the cell process [25,55]. This causes a periodic wave-like bending deformation of the axial filaments. Since these axial filaments are loaded transverse to their length and the much shorter fimbrin cross-bridging molecules are loaded axially, the primary deformation occurs in the long axial actin strands. This type of deformation is consistent with the behavior observed by Tilney and Tilney [57] in stereocilia where the fimbin linkages are flexible at attachment nodes, but do not change their length. We expect the same is true of the transverse elements in the pericellular matrix.

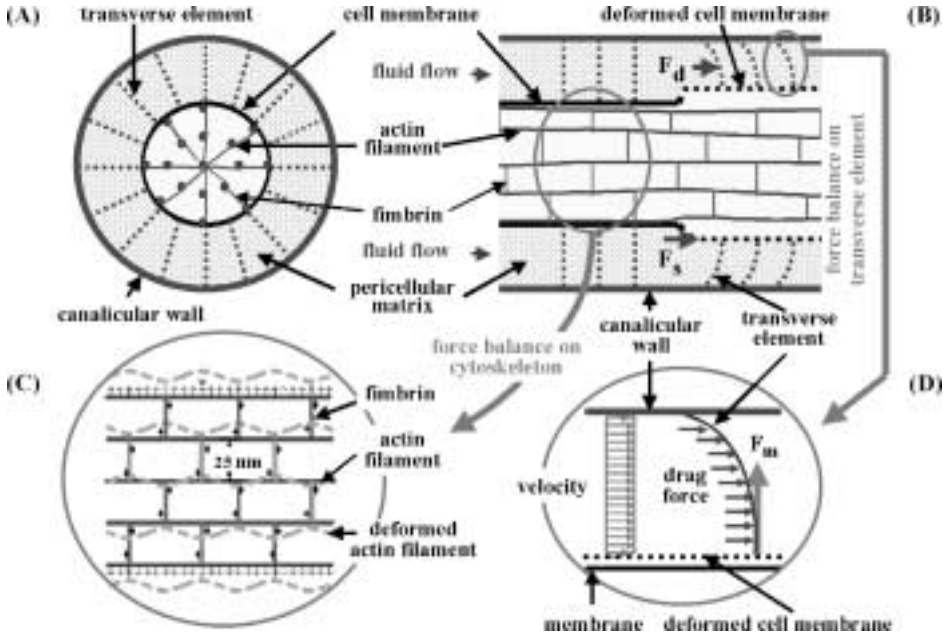

Fig. 11. Schematic model showing the structure of the pericellular matrix (PM), the intracellular actin cytoskeleton (IAC) inside the process and the connection between the PM and the IAC. (A) Transverse section of canaliculus and cell process showing the fluid annulus with transverse (radial) pericellular fibers. (B) Longitudinal section before and after the transverse elements are deformed by the flow. (C) Schematic of the cell process cytoskeletal structure in longitudinal axial section used to estimate the Young's modulus in the radial (vertical) direction. Since the length of the cell process is 300 times its radius, it is considered infinite in the longitudinal (horizontal) direction. The axial actin filaments shown are modeled as continuous infinite beams with two types of loadings depending on whether the actin filaments are peripheral or interior. The small vertical arrows indicate the direction of the loading. The (fimbrin) links between these infinitely long beams are considered to be rigid. (D) Force balance on a transverse element. Deformed shape takes the form of a catenary curve.

They deform and take the shape of a catenary curve under transverse loading (bending deformation) without significantly changing their length.

The theory for predicting the fluid flow through the pericellular matrix in the fluid annulus of the canaliculus is described in Weinbaum et al. [59]. The theory for predicting the pressure gradient along the axis of the canaliculus is based on the model in Zeng et al. [65] for flow in an osteon subject to axial loading. Combining these two theories, we are able to determine the drag force F_{d} on the transverse elements per unit cell process length and the shear force F_{s} on the cell process membrane per unit length. The ratio of these two forces, $F_{\mathrm{r}} = F_{\mathrm{d}}/F_{\mathrm{s}}$, is plotted as a function of the GAG spacing Δ in Fig. 12. This ratio is an intrinsic property of the matrix and canalicular geometry. It does not depend on the loading. One observes that for $\Delta = 7$ nm, the largest fiber spacing where the pericellular matrix could serve as a molecular sieve for albumin, the drag force is 19.6 times greater than the shear force F_{s} on the cell process membrane. The drag force is the dominant force for all values of GAG spacing in the physiological range of Δ, roughly 5–12 nm. This behavior can not be simulated in flow chamber studies since the cell process is not tethered by transverse elements to a supporting structure.

Using the theory for the hydrodynamic loading on the pericellular matrix just described, You et al. [63] have developed a non-linear model for describing the relationship between the deformation of the transverse elements in the pericellular matrix, Fig. 11D, and the deformation of the actin cytoskeleton, Fig. 11C. Rather remarkably this non-linear relationship can be expressed in closed form because the

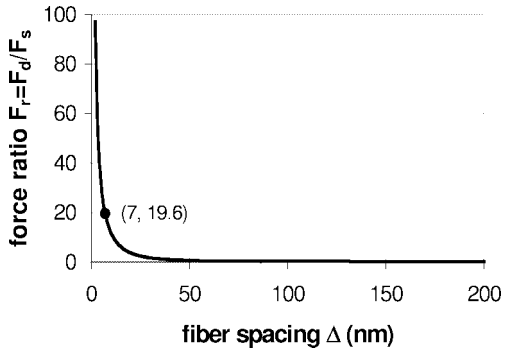

Fig. 12. The relationship between force ratio F_r and average fiber spacing Δ. Note the force ratio at $\Delta = 7$ nm is 19.6. $\Delta = 7$ nm is typical of the average spacing of GAG side chains along a core protein and the effective diameter of the albumin molecule which is known to be sieved by an equivalent matrix in capillary endothelium. Δ can vary between 5 and 12 nm. The force ratio F_r is defined as the ratio of the drag force on the fibers to the shear force on the cell process membrane per unit length of cell process.

transverse tension elements in the pericellular matrix take the shape of a simple catenary curve. Our measurements, see Fig. 10, show that the canalicular radius is approximately twice the radius of the cell process. For this typical canalicular geometry, the final relationship for the hoop strain ε_θ simplifies to

$$\beta \cdot \frac{(1+\varepsilon_\theta)}{\varepsilon_\theta} = \sinh\left[\beta \cdot \frac{(1+\varepsilon_\vartheta)(1-\varepsilon_\theta)}{\varepsilon_\theta}\right]. \tag{2}$$

Here $\beta = f_d/E^*$ is a fundamental new dimensionless group relating f_d, the drag per unit area on the transverse elements that tether the cell process to the canalicular wall, to E^*, the effective Young's modulus of the actin filament bundle.

In You et al. [63], a model based on the theory of infinitely long continuous beams is developed from first principles to determine E^* in terms of the Young's modulus E of its individual cross-linked axial actin filaments. This model is applied to the actin filament bundle sketched in Fig. 11C. The final expression for E^* is

$$E^* = 203\frac{EI}{l_2^4}, \tag{3}$$

where l_2 is the distance between cross-linking fimbrin elements and EI is the flexural rigidity of an individual actin filament. Several studies, Kishino and Yanagida [26] and Dupuis et al. [10], using different experimental techniques indicate that $EI \approx 1.5 \times 10^{-26}$ N m^2. For $l_2 = 50$ nm, this gives a value for E^* of 487 kPa. This calculated value for an actin filament bundle with five axial filaments in the centerplane of the cell process is approximately 200 times greater than the measured value for the actin gel in the cell body of an osteoblast, Shin and Athanasiou [54], where the actin filament network is isotropic and much sparser. This important result will be discussed later.

Of particular interest in this new model for the fluid drag induced strain on the cell process is the strain amplification ratio $\varepsilon_\rho = \varepsilon_\theta/\varepsilon$. Here ε is the whole bone or tissue level strain on the bone surface. These results, which are shown in Fig. 13, are obtained from Eq. (2) and the values of E^* cited above. Figure 13A shows the predictions for the strain amplification ratio and Fig. 13B the absolute strain on the cell process membrane due to the stretching of the underlying actin filament bundle. These results

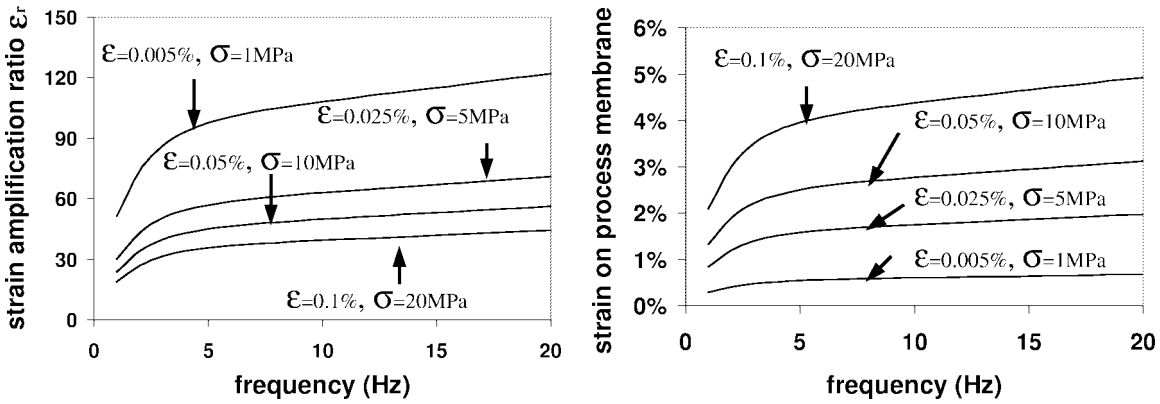

Fig. 13. Strain amplification. (A) Plot of the strain amplification ratio ε_r as a function of the load frequency for different load magnitudes. Strain amplification ratio is defined as the ratio of the hoop strain in the cell process membrane to the bone surface strain at the osteonal lumen. ε is the strain on the whole bone; σ is the load on the whole bone. (B) Plot of the cell process membrane strain ε_θ as a function of the load frequency for different load magnitudes. ε is the strain on the whole bone; σ is the load on the whole bone.

depend on the magnitude of the applied load and its frequency. The hoop strain is applied at the position of maximum flow or pressure gradient in an osteon, which the results in Zeng et al. [65] show is at the surface of the osteonal canal. The predictions in the figure can thus be viewed as an upper bound. The curves show a monotonic increase with frequency for prescribed load. The amplification ratio varies from 19 to 122 depending on load magnitude and frequency. Absolute strains from 1% to 5% are observed for loads of 5 MPa or greater. If one had used the measured value of E^* for the cell body in Shin and Athanisiou [54], one would have obtained unrealistically large cell process strains of nearly 50%.

5. Discussion

The discussion is divided into two major subsections, kidney brush border microvilli and bone cell processes. In each subsection we shall explore the new hypotheses for mechanotransduction in kidney and bone in a larger context that includes the structure and function of actin filament bundles in the intestine and hair cell stereocilia as described in the Background section.

5.1. Kidney brush border microvilli

Glomerulotubular balance was first documented using micropuncture in the rat kidney [52] where it was demonstrated that for the entire physiological range of glomerular filtration rates the fractional reabsorption of water is nearly constant. This balance is also accompanied by a “perfusion–absorption balance” in which specific solutes, such as sodium, bicarbonate and chloride ions, and glucose are found to be absorbed at rates that closely parallel the water reabsorption [8,61]. Initially, glomerulotubular balance was believed to be associated with peritubular capillary effects that derived from changes in oncotic pressure in the peritubular capillaries associated with changes in glomerular filtration rate [13,17,61] or changes in interstitial hydrostatic pressure that effected the lateral spaces and the junctions between the cells [4,15]. The inadequacy of these mechanisms to explain glomerulotubular balance was demonstrated

in a sophisticated mathematical model [60] in which the feasibility of both mechanisms was quantitatively explored. The perfusion–absorption balance was initially thought to be associated with unstirred layers within the brush border [45]. However, model calculations [2] indicate that it is unlikely that there is any convective stirring within this pile nor can the diffusion barrier within the brush border provide a significant resistance to Na^+/H^+ exchange [28].

Both glomerulotubular and perfusion-absorption balance must derive from an afferent sensor of glomerular filtration rate in series with a cascade of effector mechanisms wherein ion pumps and exchangers are activated or inserted at both the basolateral and brush border margins of the proximal tubule epithelial cells. It is well documented that the primary driving force for water movement in proximal tubule is a Na^+/K^+ exchange pump on the basolateral membrane and a Na^+/H^+ antiporter on the brush border membrane to replenish the actively transported Na^+ ions which cross the cell along its basolateral surfaces. The primary unresolved question is the identification of this afferent sensor. There is a growing body of evidence that this sensor is associated in some way with the actin cytoskeleton of the cell. Actin filaments are abundantly present both in the microvilli and the terminal web at their base [34]. This cytoskeleton has been implicated in volume regulation in several cell types [38], and, in particular, it has been shown in proximal tubule epithelia that disruption of the actin cytoskeleton prevents restorative volume regulation following hypertonic cell swelling [32]. Cantiello [7] has shown that there is a direct association between actin filament organization and the function of membrane proteins involved in transport, co-transport, ion channels and Na^+-K^+-ATPase. More recently, Lamprecht et al. [30] have shown that the Na^+/H^+ exchanger in brush border microvilli is linked via ezrin, a kinase anchoring protein, to the actin cytoskeleton. It has also been demonstrated that gross disruption of the actin filaments impairs the functioning of the proximal tubule Na^+/H^+ exchanger [29]. However, it is not known whether more subtle changes in the actin cytoskeleton that we now describe can have a controlled regulatory effect on the function of the Na^+/H^+ exchanger.

The genesis of the hypothesis in Guo et al. [16] that the proximal tubule microvilli could serve a mechanosensory function was the simple observation that these microvilli are remarkably uniform in height at the cellular level and form a highly organized hexagonal array. Such a strikingly regular organization is not necessary for transport, the main function that had been attributed to the brush border microvilli until now. The calculations presented in Figs 6, 7, and 9 lead to some very interesting new insights. First, the detailed velocity profiles in Fig. 6 provide valuable clues as to why such strict order might be necessary. We start by asking the question what would be the consequence if the microvilli were heterogeneous in height like the stereocilia in hair cells? Figure 6C shows that the velocity within the brush border is negligible, 10 nm/s, or about $1/400$ of the 4.1 μm/s slip velocity at the tips of the microvilli or brush border edge shown in Fig. 6B. However, there is a very steep velocity gradient at the brush border edge and if a microvillus were to protrude even one μm into the lumen, typical of the step height in stereocilia, one would encounter a velocity that is 150 μm/s, or 37 times the slip velocity at the brush border edge. Since the local force per unit microvillus length scales linearly with this velocity, the calculation in the next paragraph shows that this microvillus would be subject to a force, torque and tip deformation that was many times greater than its neighbors.

A rough estimate of the increase in this integrated tip force and tip deflection in the above example can be obtained by multiplying the height of the protrusion, 1 μm, by the average velocity on the protrusion, $\approx$75 μm/s, or 75 $\mu m^2/s$ and comparing this result with the corresponding calculation for a uniform microvillus. For the latter the thickness of the fiber interaction layer is only 0.18 μm and the average velocity in this layer is $\approx$2 μm/s giving a product of 0.36 $\mu m^2/s$. The drag force on the tip and hence the torque on the microvillus would be roughly $75/0.36$ or more than 200 times that of its neighbors. P_m in

Eq. (1) would increase by 200 and the deflection of the 2.5 μm microvillus in Fig. 9 would increase from 3.78 nm to 0.75 μm or 750 nm. This displacement is ten times the spacing, Δ, between the microvilli. This simple calculation shows that small heterogenieties in the height of the microvilli will cause greatly amplified displacements of the microvilli tips and that the tips would be in constant contact with one another when subject to physiological flows. The calculations in Guo et al. [16] show that these same arguments apply if the spacing, Δ, of the microvilli were not uniform. The uniformity in height and regularity of spacing are, therefore, a necessary condition to minimize the tip deflection so that each microvillus is constrained in its motion to a localized region about its equilibrium position and adjacent tips do not interact. If tip interaction between adjacent microvilli were important, it would seem that there would be tip and lateral links between microvilli as found in the hair cell stereocilia sketched in Fig. 1. Presently, there is no evidence for this.

The above calculation when compared with the measured deformation of hair cell stereocilia provides a very striking contrast. The total drag force on a uniform microvillus when $Q = 30$ nl/min, as noted previously, is only 0.0074 pN. Roughly $3/4$ of this total force, or 0.0055 pN, occurs in the interaction layer at the microvillus tip. As calculated in the previous paragraph this force would be magnified 200 fold and increase to 1.1 pN if it protruded one micron above its neighbors. However, even a 1.1 pN force is small compared to the 100 pN forces that are applied at the tip of the tallest stereocilia in eliciting a depolarization response in a hair cell bundle. Typical displacements in the tallest stereocilia required to open cationic ion channels in the vicinity of the tip link in a hair cell bundle vary from 10 to 100 nm, see Fig. 1. However, the interconnected microvilli in a hair bundle form a much stiffer structure. The core of the stereocilia, though typically only two to three times the 90 nm diameter of a kidney microvillus, contains several hundred actin filaments [57] and the stereocilia themselves are connected by stiff lateral links both along and across rows near their apex, which do not appear to extend under tension [24]. Thus, the entire hair cell bundle consisting of 50–100 stereocilia in each hair cell must respond when a force is applied to just the tallest stereocilia. This structure would be extremely stiff were it not for the fact that the stereocilia greatly taper as they enter the cuticular plate and are able to bend about their ankles where the number of actin filaments is reduced from several hundred to 20–30. In contrast to this much stiffer interconnected structure, the kidney microvillus in our model has only seven actin filaments and, to the best of our knowledge, is not connected to any of its neighbors by lateral linkages. It is, therefore, not unreasonable that a one pN force applied at its tip could produce a 750 nm deflection, as estimated above.

Are the predicted small deflections of the microvilli tips shown in Fig. 9 sufficient for a mechano-electrical response similar to the depolarization/hyperpolarization response observed in hair cells? This would seem unlikely, not because the deflections are small for a highly uniform microvillus array, but because in hair cells the elastic gating mechanism for the stereocilia is a localized stretching of the membrane above the dense zone in the vicinity of the tip link, see Fig. 1. In the absence of tip links this type of interaction would not seem possible. The critical question in kidney microvilli is how the small predicted tip deflections in Fig. 9 can produce a large enough signal for the cytoskeleton in the cell body to respond? One needs either a major amplification of strain or force applied to the actin cytoskeleton. How does this arise?

If the microvilli are truly uncoupled then each microvillus acts as if it were a tall tree in a dense forest whose tops are blowing in the wind. The tree will experience its largest deflections at its top but is usually toppled by the large torque exerted on its roots. We believe the secret to the cytoskeletal amplification is the force experienced by the actin filaments at the roots of the microvillus where it is fastened to the supporting structure in its terminal web, see Fig. 3. To determine this amplification let us return to Fig. 8A

and consider the moment about the three central actin filaments in the midplane of the actin bundle at its base. This resisting moment must balance the torque about the base of the microvillus due to its hydrodynamic loading. As noted in Fig. 7, 86% of this total torque is due to the contribution $P_{\mathrm{m}}L$ arising from the tip layer interaction. This torque is resisted by the four off axis actin filaments in Fig. 8A. Two of the actin filaments are in tension and two are in compression and the lever arm about the three central filaments is $\sqrt{3}a/4$. If the force on each actin filament is P_{t}, where the subscript t stands for terminal web, the total resisting moment at the base is $\sqrt{3}P_{\mathrm{t}}a$. Neglecting for the moment the contribution that arises from the distributed loading q_{m} in the brush border, one finds that if this moment is to resist the hydrodynamic torque at the microvillus tip, $P_{\mathrm{t}} = (P_{\mathrm{m}}L)/(\sqrt{3}a)$, a in our model is assumed to be 45 nm whereas L is 2500 nm. The force on the actin filaments at the base of the microvillus is amplified by a factor of 32 and, if the additional torque due to the distributed force q_{m} in the brush border is also included, this amplification factor increases to 38. Although the drag on the microvillus tip, P_{m}, is only 0.0055 pN, the force on the microfilaments at the microvillus base are 38 times this or 0.2 pN.

The 0.41 pN force just calculated is typical of the forces applied by optical tweezers in moving a protein laterally in the plane of the membrane when it is attached to a small bead in a laser trap. A force of 0.5 pN is required to produce a large deformation in a single actin filament strand in the microdomain fence model of Sako and Kusumi [48] for the restricted diffusion of proteins in the membrane of the bilayer. A 1.0 pN force is sufficient to release the bead-protein complex from its optical trap at the border of a microdomain. It is also obvious that if the microvilli were non-uniform in height, the forces on the microfilaments at their base would be so large that the supporting structure would easily buckle. P_{m} would increase 200 fold to 1.1 pN and P_{t} would be 38 times this, or 42 pN.

While the drag force on an individual microvillus is very small, their density, 42.5 /μm^2 in rat proximal tubule, is quite large with the result that there are typically 4×10^3 per cell and the total drag is approximately 30 pN at $Q = 30$ nl/min. This drag is about one order of magnitude less than the integrated shear force on an endothelial cell whose surface area is 300 μm^2 at a shear stress of 10 dyn/cm^2, where a variety of intracellular responses have been observed for cell cultures in flow chambers [44,62]. The collective behavior of all the microvilli is, thus, marginal for eliciting the equivalent of a shear stress response. These forces which act over the entire surface of a cell are two orders of magnitude smaller than the traction force on locomoting cells where adhesive integrins play an important role [41]. One can only speculate why the small deformations due to fluid shear and fluid drag forces can cause important biological responses where they are so small compared to the force a cell can generate itself on a substrate.

The foregoing predictions demonstrate the quantitative feasibility of the kidney microvilli acting as a mechanotransducer for the sensing of flow. The model provides a rational explanation as to why the microvilli are so uniform in height and spacing and also provides an amplification mechanism that is required if the small drag forces acting on the microvilli tips are be transmitted as much larger tensile and compressive forces acting on the cytoskeletal elements in the terminal web region of the microvillus. The requirements of this mechanosensory system would appear to require that the microvilli behave as relatively stiff bristles which are capable of small deflections wherein each microvillus does not interact with its neighbors, in sharp contrast to hair cell stereocilia.

A relatively simple critical experiment can be performed to test this basic hypothesis, namely, to alter the viscosity of the glomerular filtrate, but maintain the same flow rate in the tubule. This experiment is most easily conducted on a single perfused tubule in which the viscosity of the perfusing fluid is increased. The increase in viscosity of the perfusate should increase the drag on the microvillus tip although the flow is maintained constant. Although the hydrodynamic drag and hence the torque on the

microvillus increases linearly with the viscosity, one should not expect a linear response for an isolated tubule. The experiments in [36] have shown that at increased flow rates the separation between microvilli increases substantially. This is due to the increase in pressure in the tubule lumen which causes a dilation of its diameter. This same type of behavior will ensue in a single perfused tubule in which the filtrate viscosity is increased. To maintain a constant flow rate while increasing the viscosity one must increase the lumen pressure and hence also dilate the lumen of the tubule. Nevertheless, one would expect to see an increase in reabsorption as the viscosity is increased. This increase should be less than linear since Fig. 5 in Guo et al. [16] shows that the dimensionless drag coefficient decreases as the spacing between the microvilli increases. Preliminary experiments are currently being performed by T. Wang at Yale University to test this hypothesis.

5.2. Bone cell processes

The model in You et al. [63] examines for the first time the effect of hydrodynamic drag forces on extracellular matrix and the effect of the resulting deformation of this matrix on the strains produced in a cell's actin cytoskeleton. The results in Fig. 13 suggest that the small mechanically induced strains on whole bone at physiological loading can be greatly amplified at the cellular cytoskeletal level if the fluid drag forces on the pericellular matrix are transmitted to the actin filament bundles in the cell process. Furthermore, the theoretical predictions in Fig. 13B reveal that this amplification can lead to strains in a range where intracellular biochemical responses have been observed in cell culture systems.

In the past, researchers examining the effect of fluid flow on cells without microvilli and cell processes have focused their attention nearly exclusively on the response of cells to fluid shear stress. The effect of drag forces exerted on extracellular matrix fibers has not previously been considered because the flow through the matrix and the resulting drag forces are very small compared to the shearing force applied at the edge of the matrix layer. In contrast, in bone cell canaliculi the fluid must pass through the pericellular matrix since this matrix fills the entire fluid annulus and is tethered to the canalicular wall. The fascinating prediction in Fig. 12 is that the drag force on this tethered matrix per unit length of cell process is $\approx$20 times greater than the shear force acting on a unit length of cell process membrane. The distributed force on the pericellular matrix fibers is thus much larger than the shear force on the cell process membrane itself. However, all current experiments examining the effect of fluid forces on bone cells look at the effect of fluid shear rather than fluid drag. The results in Fig. 12 for the relative importance of fluid drag compared to fluid shear are a property of the canalicular and cell process geometry and the GAG spacing. In Fig. 12, this spacing has been taken as 7 nm so that the matrix can also serve as a molecular filter for molecules the size of albumin (7 nm effective diameter) or larger.

As mentioned in the introduction, many investigators have accepted the hypothesis proposed in Weinbaum et al. [59] that fluid shear stress is the stimulus for intracellular biochemical response in bone cells. This is based on the non-intuitive prediction in Weinbaum et al. [59] that the fluid shear stress on the cell process membrane due to mechanical loading is roughly of the same magnitude, 5–30 dyn/cm^2, as the fluid shear stresses on vascular endothelial cells. Moreover, the same types of biochemical responses observed for endothelial cells at shear stresses in this range are also observed for bone cells [44,62]. However, there is a fundamental difference between these two cell types that has not previously been considered. The actin filament bundles in bone cell processes have a predicted effective elastic modulus $E^* = 487$ kPa which is 200 times greater than the 2.5 kPa modulus measured in Shin and Athanasiou [54] for bone cells. The latter modulus is for the actin gel in the cell body rather than the actin filament bundles in the cell processes which we propose are the actual sensing sites of mechanical forces and

strains *in vivo*. Bone cells may behave in a similar manner to endothelial cells when subjected to fluid shear, but the present analysis suggests that this is a response of the cell body as opposed to a response of the bone cell processes, which are much stiffer.

In view of this new insight, it would appear that the more meaningful *in vitro* mechanical experiments for bone cells are cell culture studies in which bone cells are stretched on elastic substrates. In these experiments the strain levels required to produce a cellular response are 1–10% [5,39]. Strain levels produced in four point bending experiments are significantly lower, 0.38% [43]. The latter strains are at the very upper limit of the peak level of strains on whole bone which range from about 0.04–0.2% in humans under varied activities [6,31] and 0.04–0.3% for animal locomotion [11]. The strain levels achieved in *in vitro* cell culture studies are much greater than the whole tissue strains experienced physiologically *in vivo*. Klein-Nulend et al. [27] and You et al. [64] have shown that when physiological strains of less than one percent are applied in cell culture, there is no observed cellular response. The rapid increase in NO production observed by Pittsillides in four point bending is at the extreme of physiological loading. These observations have cast doubt on any previous theory that proposed that cell stretch is a viable candidate for cell activation in bone.

The predictions in Fig. 13 and the new strain amplification process proposed in You et al. [63] and illustrated in Fig. 11, provide the first rational basis for explaining this important conundrum. Our model predicts that whole bone strains can be amplified by a factor of 20–100 or more and that the resulting absolute strains, 0.3–5%, are, indeed, in the range where biological responses have been observed. The analysis also brings to light a new fundamental dimensionless parameter $\beta = f_{\mathrm{d}}/E^*$ relating the drag force on the pericellular matrix to the effective elastic modulus of the actin filament bundle in the cell process. The elastic properties of the pericellular matrix do not appear in Eq. (2) since the stiffness of the tethering elements in the pericellular matrix is assumed to be small compared to the filaments in the actin bundle that form the core of the cell process. The neglect of the bending stiffness of these transverse elements allows one to obtain a simplified catenary shape for the transverse tethering filaments. The identity of these filaments is unknown, but the recent study by Henry and Duling [20] of the matrix on endothelial cells suggests that this molecule may be hyaluronan.

The models for the kidney microvilli and the bone cell process provide an interesting contrast. In both cases one is hard put to explain how very small deformations can lead to a cytoskeletal signal that exceeds some threshold. In the kidney the predicted deformations of the microvilli are very small, certainly too small for the activation of ion channels as in the case of stereocilia. The amplification we propose arises from the huge mechanical advantage that results from the fact that the actin filament bundle in the microvillus serves as a long lever arm which produces vastly greater forces on the actin filaments at the base of the microvillus than the hydrodynamic forces at its tip. The axial actin filament bundle is securely fastened to the matrix elements in the terminal web of the cytoskeleton beneath the apical surface, much like the roots of a tree. In bones it is the tissue level strains that are too small and a large amplification in strain is needed at the cellular level for the bone cells to sense these small mechanical deformations. The interesting prediction here, is that although the actin filament bundle in the cell process is much stiffer than the actin gel in the cell body of the osteocyte, it is still sufficiently elastic to experience significant hoop strains that are much larger than whole bone tissue strains. Very little is known about the terminal web of the cell process, but it seems very unlikely that it can function in a manner than is similar to a microvillus. The fluid flow is along the axis of the cell process, rather than transverse to it, and it can experience little bending deformation since it is tethered to the canalicular wall along its entire length.

What is curious about this comparative analysis of actin filament bundles in various tissues is that the basic structure of the bundle itself does not appear to be that dissimilar and yet this same basic structure can function so differently in each tissue. One puzzling question that the authors have not been able to answer is why the brush border microvilli in the intestine have a regularity in height and spacing that is quite similar to kidney microvilli. We have developed a strong rational argument in this paper for why this highly ordered structure is critical for the functioning of the kidney microvilli as a mechanotransducer, but it is not at all apparent why such regularity in structure is needed in the intestine.

Acknowledgement

The authors wish to thank their colleagues S. Cowin, M. Schaffler and A. Weinstein for enlightening discussions which that led to the new hypotheses that are described in Guo et al. (2000) and You et al. (2001) that were the genesis for this more inclusive comparative study of cells with actin filament bundles. L. You also wishes to thank S. Henderson, D. Laudier and V.A. Williams at the Mount Sinai School of Medicine for their invaluable assistance in obtaining the electron micrographs that are shown in this paper. This research has been supported by NIH grant R01-AR44211.

References

[1] E.M. Aarden, A.M. Wassenaar, M.J. Alblas and P.J. Nijweide, Immunocytochemical demonstration of extracellular matrix proteins in isolated osteocytes, *Histochem. Cell Biol.* **106** (1996), 495–501.
[2] D. Basmadjian, D.S. Dykes and A.D. Baines, Flow through brush borders and similar protuberant wall structures, *J. Membr. Biol*. **56** (1980), 183–190.
[3] M. Bendayan, Ultrastructural localization of actin in muscle, epithelial and secretory cells by applying the protein A-gold immunocytochemical technique, *Histochem. J.* **15** (1983), 39–58.
[4] B.M. Brenner, K.H. Falchuk, R.I. Keimowitz and R.W. Berliner, The relationship between peritubular capillary protein concentration and fluid reabsorption by the renal proximal tubule, *J. Clin. Invest.* **48** (1969), 1519–1531.
[5] E.H. Burger and J.P. Veldhuijzen, Influence of mechanical factors on bone formation, resorption, and growth *in vitro*, in: *Bone*, B.K. Hall, ed., Vol. 7, CRC Press, Boca Raton, FL, 1993, pp. 37–56.
[6] D.B. Burr, C. Milgrom, D. Fyhrie, M. Forwood, M. Nyska, A. Finestone, S. Hoshaw, E. Saiag and A. Simkin, In vivo measurement of human tibial strains during vigorous activity, *Bone* **18** (1996), 405–410.
[7] H.F. Cantiello, Role of actin filament organization in cell volume and ion channel regulation, *J. Exp. Zool.* **279** (1997), 425–435.
[8] Y.L. Chan, B. Biagi and G. Giebisch, Control mechanisms of bicarbonate transport across the rat proximal convoluted tubule, *Am. J. Physiol.* **242** (1982), F532–F543.
[9] S.C. Cowin, S. Weinbaum and Y. Zeng, A case for bone canaliculi as the anatomical site of strain generated potentials, *J. Biomech.* **28** (1995), 1281–1297.
[10] D.E. Dupuis, W.H. Guilford, J. Wu and D.M. Warshaw, Actin filament mechanics in the laser trap, *J. Muscle Research and Cell Motility* **18** (1997), 17–30.
[11] S.P. Fritton, J.M. Kenneth and C.T. Rubin, Quantifying the strain history of bone: spatial uniformity and self-similarity of low magnitude strains, *J. Biomech.* **33** (2000), 317–325.
[12] R. Furukawa and M. Fechheimer, The structure, function, and assembly of actin filament bundles, *Int. Rev. Cytol.* **175** (1997), 29–90.
[13] K.H. Gertz and J.W. Boylan, Glomerular-tubular balance, in: *Handbook of Physiology*, Section 8: Renal Physiology, J. Orloff and R.W. Berliner, eds, American Physiological Society, Washington, DC, 1973, pp. 763–790.
[14] A.R. Gohel, A.R. Hand and G.A. Gronowicz, Immunogold localization of beta 1-integrin in bone: effect of glucocorticoids and insulin-like growth factor I on integrins and osteocyte formation, *J. Histochem. Cytochem.* **43** (1995), 1085–1096.
[15] R. Green, E.E. Windhager and G. Giebisch, Protein oncotic pressure effects on proximal tubular fluid movement in the rat, *Am. J. Physiol.* **226** (1974), 265–276.
[16] P. Guo, A. Weinstein and S. Weinbaum, A hydrodynamic mechanosensory hypothesis for brush border microvilli, *Am. J. Physiol. Renal Physiol.* **279** (2000), F698–F712.

[17] D.A. Haberle and H. von Baeyer, Characteristics of glomerulotubular balance, *Am. J. Physiol.* **244** (1983), F355–F366.
[18] C.M. Hackney and D.N. Furness, Mechanotransduction in vertebrate hair cells: structure and function of the stereociliary bundle, *Am. J. Physiol.* **268** (1995), C1–13.
[19] O.E. Hassen and L. Hermann. The presence of an axial structure in the microvillus of the mouse convoluted proximal tubule cell, *Lab. Invest.* **11** (1962), 610–616.
[20] C.B. Henry and B.R. Duling, Permeation of the luminal capillary glycocalyx is determined by hyaluronan, *Am. J. Physiol.* **277** (1999), H508–H514.
[21] J. Howard and A.J. Hudspeth, Mechanical relaxation of the hair bundle mediates adaptation in mechanoelectrical transduction by the bullfrog's saccular hair cell, *Proc. Natl. Acad. Sci.* **84** (1987), 3064–3068.
[22] A.J. Hudspeth, Models for mechanoelectrical transduction by hair cells, *Prog. Clin. Biol. Res.* **176** (1985), 193–205.
[23] A.J. Hudspeth, Hair-bundle mechanics and a model for mechanoelectrical transduction by hair cells, *Soc. Gen. Physiol. Ser.* **47** (1992), 357–370.
[24] B. Kachar, F. Liang, U. Lins, M. Ding, X.R. Wu, D. Stoffler, U. Aebi and T.T. Sun, Three-dimensional analysis of the 16 nm urothelial plaque particle: luminal surface exposure, preferential head-to-head interaction, and hinge formation, *J. Mol. Biol.* **285** (1999), 595–608.
[25] G.J. King and M.E. Holtrop, Actin-like filaments in bone cells of cultured mouse calvaria as demonstrated by binding to heavy meromyosin, *J. Cell Biology* **66** (1975), 445–451.
[26] A. Kishino and A. Yanagida, Force measurements by micro manipulation of a single actin filament by glass needles, *Nature* **334** (1988), 74–76.
[27] J. Klein-Nulend, A. van der Plas, C.M. Semeins, N.E. Ajubi, J.A. Frangos, P.J. Nijweide and E.H. Burger, Sensitivity of osteocytes to biomechanical stress in vitro, *FASEB J.* **9** (1995), 441–445.
[28] T.A. Krahn and A.M. Weinstein, Acid/base transport in a model of the proximal tubule brush border: impact of carbonic anhydrase, *Am. J. Physiol.* **270** (1996), F344–F355.
[29] K. Kurashima, S. D'Souza, K. Szaszi, R. Ramjeesingh, J. Orlowski and S. Grinstein, The apical Na^+/H^+ exchanger isoform NHE3 is regulated by the actin cytoskeleton, *J. Biol. Chem.* **274** (1999), 29 843–29 849.
[30] G. Lamprecht, E.J. Weinman and C.-H.C. Yun, The Role of NHERF and E3KARP in the cAMP-mediated inhibition, *J. Biol. Chem.* **273** (1998), 29 972–29 978.
[31] L.E. Lanyon, W.G. Hampson, A.E. Goodship and J.S. Shah, Bone deformation recorded in vivo from strain gauges attached to the human tibial shaft, *Acta Orthop. Scand.* (1975), 256–268.
[32] M.A. Linshaw, C.A. Fogel, G.P Downey, E.W.Y. Koo and A.I. Gotlieb, Role of cytoskeleton in volume regulation of rabbit proximal tubule in dilute medium, *Am. J. Physiol.* **262** (1992), F144–F150.
[33] D. Louyard, The function of the major cytoskeletal components of the brush border, *Curr. Opin. Cell. Biol.* **1** (1989), 51–57.
[34] A.B. Maunsbach and E.I. Christensen, Functional ultrastructure of the proximal tubule, in: *Handbook of Physiology*, Section 8, Chapter 2: Renal Physiology, E.E. Windhager, ed., Oxford Univ. Press, New York, 1992, pp. 41–107.
[35] A.B. Maunsbach, G.H. Giebisch and B.A. Stanton, Effects of flow rate on proximal tubule ultrastructure, *Am. J. Physiol.* **253** (1987), F582–F587.
[36] A.B. Maunsbach, Ultrastructure in the proximal tubule, in: *Handbook of Physiology*, Renal Physiology, Section 8, Chapter 2, J. Orloff, R.W. Berliner and S.R. Geiger, eds, American Physiological Society, Washington, DC, 1973, pp. 31–79.
[37] M.S. Mooseker and L.G. Tilney, Organization of an actin filament–membrane complex. Filament polarity and membrane attachment in the microvilli of intestinal epithelial cells, *J. Cell Biol.* **67** (1975), 725–743.
[38] A. Moustakas, P.A. Theodoropoulos, A. Gravanis, D. Haussinger and C. Stournaras, The cytoskeleton in cell volume regulation, *Contrib. Nephrol.* **123** (1998), 121–134.
[39] D.W. Murray and N. Rushton, The effect of strain on bone cell prostaglandin E2 release: a new experimental method, *Calcif. Tissue Int.* **47** (1990), 35–39.
[40] H. Nakamura, S. Kenmotsu, H. Sakai and H. Ozawa, Localization of CD44, the hyaluronate receptor, on the plasma membrane of osteocytes and osteoclasts in rat tibiae, *Cell Tissue Res.* **280** (1995), 225–233.
[41] T. Oliver, M. Dembo and K. Jacobson, Traction forces in locomoting cells, *Cell Motility and the Cytoskeleton* **31** (1995), 225–240.
[42] J.O. Pickles, A model for the mechanics of the stereociliar bundle on acousticolateral hair cells, *Hear Res.* **68** (1993), 159–172.
[43] A.A. Pitsillides, S.C. Rawlinson, R.F. Suswillo, S. Bourrin, G. Zaman and L.E. Lanyon, Mechanical strain-induced NO production by bone cells: a possible role in adaptive bone (re)modeling?, *FASEB J.* **9** (1995), 1614–1622.
[44] K.M. Reich and J.A. Frangos, Effects of flow on prostaglandin E2 (PGE2) and inositol trisphosphate (IP3) levels in osteoblasts, *Am. J. Physiol.* **261** (1991), C428–C432.
[45] I.W. Richardson, V. Licko and E. Bartoli, The nature of passive flows through tightly folded membranes, *J. Membr. Biol.* **11** (1973), 293–308.

[46] J.S. Rodman, M. Mooseker and M.G. Farquhar, Cytoskeletal proteins of the rat kidney proximal tubule brush border, *Eur. J. Cell Biol.* **42** (1986), 319–327.
[47] J. Rostgaard and L. Thuneberg, Electron microscopic observation the brush border of proximal tubule cells of mammalian kidney, *Z. Zellforsch.* **132** (1972), 473–496.
[48] Y. Sako and A. Kusumi, Barriers for lateral diffusion of transferrin receptors in the plasma membrane as characterized by receptor dragging by laser tweezers: fence versus tethering, *J. Cell Biol.* **129** (1995), 1559–1574.
[49] R.A. Salzstein and S.R. Pollack, Electromechanical potentials in cortical bone-II. Experimental analysis, *J. Biomech.* **20** (1987), 271–280.
[50] A.S. Sangani and A. Acrivos, Slow flow past periodic array of cylinders with application to heat transfer, *J. Multiphase Flow.* **8**(3) (1982), 193–206.
[51] Y.M.H.F. Sauren, R.H.P. Mieremet, C.G. Groot and J.P. Scherft, An electron microscopic study on the presence of proteoglycans on the mineralized matrix of rat and human compact lamellar bone, *The Anatomical Record* **232** (1992), 36–44.
[52] J. Schnermann, M. Wahl, G. Liebau and H. Fischbach, Balance between tubular flow rate and net fluid reabsorption in the proximal convolution of the rat kidney, *Pf. Arch.* **304** (1968), 90–103.
[53] G.C. Scott and E. Korostoff, Oscillatory and step response electromechanical phenomena in human and bovine bone, *J. Biomech.* **23** (1990), 127–143.
[54] D. Shin and K. Athanasiou, Cytoindentation for obtaining cell biomechanical properties, *J. Orthop. Res.* **17** (1999), 880–890.
[55] K. Tanaka-Kamioka, H. Kamioka, H. Ris and S.S. Lim, Osteocyte shape is dependent on actin filaments and osteocyte processes are unique actin-rich projections, *J. Bone Mineral Res.* **13**(10) (1998), 1555–1568.
[56] L.G. Tilney, M.S. Tilney and D.A. Contanche**,** Action filaments Stereocilia and hair cells of the bird cochlea. V. How the stair case stereociliary lengths is generated, *J. Cell Biol.* **106** (1988), 355–365.
[57] L.G. Tilney and M.S. Tilney, Functional organization of the cytoskeleton, *Hear Res*. **22** (1986), 55–77.
[58] F. Wassermann and J.A. Yaeger, Fine structure of the osteocyte capsule and of the wall of the lacunae in bone, *Zeitschrift für Zellforschung* **67** (1965), 636–652.
[59] S. Weinbaum, S.C. Cowin and Y. Zeng, A model for the excitation of osteocytes by mechanical loading-induced bone fluid shear stresses, *J. Biomech.* **27** (1994), 339–360.
[60] A.M. Weinstein, Glomerulotubular balance in a mathematical model of the proximal nephron, *Am. J. Physiol.* **258** (1990), F612–F626.
[61] C.S. Wilcox and C. Baylis, Glomerular-tubular balance and proximal regulation, in: *The Kidney. Physiology and Pathophysiology*, D.W. Seldin and G. Giebisch, eds, Raven Press, New York, 1985, pp. 985–1012.
[62] J.L. Williams, J.P. Iannotti, A. Ham, J. Bleuit and J.H. Chen, Effects of fluid shear stress on bone cells, *Biorheology* **31** (1994), 163–170.
[63] L.D. You, S.C. Cowin, M.B. Schaffler and S. Weinbaum, Flow induced cytoskeletal strain amplification: Turning up the strain in bone cells, *J. Biomech.* (2001), in review.
[64] J. You, C.E. Yellowley, H.J. Donahue, Y. Zhang, O. Chen and C.R. Jacobs, Substrate deformation levels associated with routine physical activity are less stimulatory to bone cells relative to loading-induced oscillatory fluid flow, *J. Biomech. Eng.* **122** (2000), 387–393.
[65] Y. Zeng, S.C. Cowin and S. Weinbaum, A fiber matrix model for fluid flow and streaming potentials in the canaliculi of an osteon, *Ann. Biomed. Eng.* **22** (1994), 280–292.
[66] D. Zhang, S.C. Cowin and S. Weinbaum, Electrical signal transmission and gap junction regulation in a bone cell network: A cable model for an osteon, *Ann. Biomed. Eng.* **25** (1997), 379–396.